LETTERS

Spatiotemporal dynamics of RhoA activity in migrating cells

Olivier Pertz[1,2]†, Louis Hodgson[1,2]†, Richard L. Klemke[2]† & Klaus M. Hahn[1,2]†

Rho family GTPases regulate the actin and adhesion dynamics that control cell migration. Current models postulate that Rac promotes membrane protrusion at the leading edge and that RhoA regulates contractility in the cell body[1,2]. However, there is evidence that RhoA also regulates membrane protrusion[3,4]. Here we use a fluorescent biosensor, based on a novel design preserving reversible membrane interactions, to visualize the spatiotemporal dynamics of RhoA activity during cell migration. In randomly migrating cells, RhoA activity is concentrated in a sharp band directly at the edge of protrusions. It is observed sporadically in retracting tails, and is low in the cell body. RhoA activity is also associated with peripheral ruffles and pinocytic vesicles, but not with dorsal ruffles induced by platelet-derived growth factor (PDGF). In contrast to randomly migrating cells, PDGF-induced membrane protrusions have low RhoA activity, potentially because PDGF strongly activates Rac, which has previously been shown to antagonize RhoA activity[5,6]. Our data therefore show that different extracellular cues induce distinct patterns of RhoA signalling during membrane protrusion.

To study the spatiotemporal dynamics of RhoA activation in living cells, we designed a genetically encoded, single-chain biosensor with intramolecular fluorescence resonance energy transfer (FRET) that responds to RhoA activation. As depicted in Fig. 1a, the biosensor consists of a Rho-binding domain of the effector rhotekin (RBD, amino acids 7–89), which specifically binds to GTP·RhoA[7], followed by cyan fluorescent protein (CFP), an unstructured linker of optimized length, a pH-insensitive variant of yellow fluorescent protein[8] (YFP), and full-length RhoA. Upon activation by GTP-loading, the RBD binds to Rho, modifying the relative orientation of the two fluorophores and thereby increasing FRET. Because the fluorescent proteins are attached to one another, RhoA activation can be approximated simply as being proportional to the FRET/CFP emission ratio at a given subcellular location[9]. The two fluorophores are placed on the internal portion of the biosensor chain, leaving the carboxy terminus of RhoA intact for binding to Rho guanosine dissociation inhibitor[10] (RhoGDI). This important regulatory interaction controls reversible membrane localization.

As the size of the biosensor precluded purification for *in vitro* characterization, we analysed the fluorescence spectra of mutant biosensors expressed in suspensions of living HEK-293T cells. G14V and Q63L dominant-positive mutants showed higher emission ratios than a T19N dominant-negative or an F39A effector binding mutant unable to interact with the RBD[7] (Fig. 1b, c). Notably, the emission ratios of the wild-type and dominant-positive biosensors were similar (Fig. 1b, c). This is due to the high biosensor expression level required to obtain a reasonable signal-to-noise ratio in this assay (more than an order of magnitude above endogenous RhoA levels, Supplementary Fig. S1a). At this concentration, there is insufficient endogenous RhoGDI to prevent the biosensor from accumulating at the plasma membrane (Supplementary Fig. S1b), where it can be activated by guanine nucleotide exchange factors (GEFs). Emission ratios of wild-type biosensor were reduced by co-expression of RhoGDI, p50 Rho GTPase activating protein (GAP) or C3-transferase, but not by Rap GAP, which does not interact with RhoA (Fig. 1c). To test the ability of the biosensor to respond to GEFs, we first sequestered it in the cytosol by co-expressing RhoGDI. Co-expression of truncated, constitutively active GEFs that can activate RhoA (Dbl and Ect2) rescued the high emission ratio and membrane localization, whereas GEFs that do not interact with RhoA (Tiam1

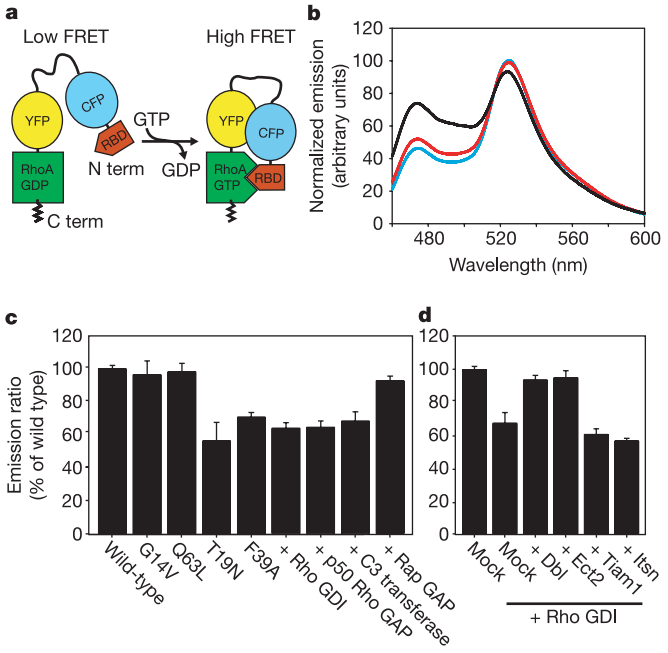

Figure 1 | Design and characterization of the RhoA biosensor. a, Probe design. **b**, Normalized emission spectra of biosensor mutants expressed in HEK-293T cells (excitation at 433 nm). Blue, wild-type biosensor; red, Q63L dominant-positive biosensor; black, T19N dominant-negative biosensor. **c**, **d**, Normalized FRET/CFP emission ratios: mutant RhoA biosensors and wild-type biosensor co-expressed with negative regulators (**c**) or GEFs (**d**) as shown. Results are the mean of at least three independent measurements. Error bars represent standard deviations; $P < 0.001$ (*t*-test) for differences between wild type and signals from T19N, F39A, +Rho GDI, +p50 Rho GAP, +C3 transferase (in **c**) and +Rho GDI, +Tiam1, +Itsn (in **d**).

[1]University of North Carolina at Chapel Hill, Department of Pharmacology and Lineberger Cancer Center, Chapel Hill, North Carolina 27599, USA. [2]Department of Cell Biology, The Scripps Research Institute, 10550 North Torrey Pines Road, La Jolla, California 92037, USA. †Present addresses: University of California at San Diego, Department of Pathology and Moores Cancer Center, Basic Science Building, Room 1040, 9500 Gilman Drive, MC 0612, La Jolla, California 92093, USA (O.P., R.L.K.); University of North Carolina at Chapel Hill, Department of Pharmacology and Lineberger Cancer Center, Chapel Hill, North Carolina 27599, USA (L.H., K.M.H.).

and intersectin) had no effect (Fig. 1d and Supplementary Fig. S1b). Efficient co-expression of these constructs was verified by western blotting (Supplementary Fig. S1c).

For live-cell imaging, we developed a tetracycline-inducible mouse embryonic fibroblast (MEF) cell line that enabled biosensor expression at levels similar to endogenous RhoA, at which RhoGDI binding capacity is not overwhelmed and cell morphology and motile behaviour are not altered (Supplementary Movie S1). Further characterization of the biosensor in the MEF and HEK-293T cell systems is presented in the Supplementary Information. In non-motile cells (plated on fibronectin overnight), RhoA activity was always much higher at the periphery than in the cell body (Supplementary Fig. S5b). We observed a previously undescribed perinuclear accumulation of RhoA that colocalizes with a Golgi marker (Supplementary Fig. S5b). This pool of RhoA consistently showed among the lowest activation values in the cell. The significance of an inactive, Golgi-resident pool of RhoA is unclear. However, the Golgi-resident protein ARAP1 (ref. 11) has GAP activity for RhoA and may inactivate it at this location. ARAP1 also regulates Arf1, suggesting that this compartment may serve as a platform for the previously documented crosstalk between RhoA and Arf1[12].

We next examined the localization of RhoA activation in MEF cells randomly migrating on fibronectin (optimal motile behaviour was observed six hours after re-plating). Activation was consistently observed wherever protrusions were extending (Fig. 2a, c and Supplementary Movies S2, S3). There was a sharp band of markedly higher activity immediately adjacent to the cell edge (Fig. 2b, d), superimposed on a broader gradient of lower activation decreasing from the edge of the cell inwards. This was observed in 17 out of 19 protrusions ($n = 10$ cells), and was also found in cells migrating out of a wounded monolayer (data not shown). RhoA activity was infrequently observed during tail retraction. However, activation was obvious when such contractile behaviour was very robust (Fig. 2f, g; $n = 5$ cells). Only minimal RhoA activity was found in the cell body.

As an independent measure of RhoA activation in cell protrusions, we isolated pseudopods extending towards a gradient of fibronectin using a recently described technique[13]. Rhotekin pull-down assays showed that RhoA activity was higher in pseudopods than in the cell body (Fig. 2e). In this assay, Erk2 has been shown to be equally distributed in the pseudopod and body fractions, and serves as a loading control. Further pointing to a role for RhoA in membrane protrusion, low-level expression of dominant-negative T19N GFP–RhoA or T19N biosensor produced cells with concave edges that were unable to produce lamellae (Supplementary Fig. S3a). High expression of this mutant led to cell detachment (data not shown). Previous studies are consistent with roles for RhoA effectors directly at the leading edge, including adducin phosphorylation by Rho kinase[3] (ROK), stabilization of microtubules by diaphanous-related formin (mDia)[4], and potentially ROK-dependent myosin phosphorylation in a broader region throughout the lamellipod[14]. At the cell rear, RhoA might interact with ROK to turn on myosin[15] during robust contractile events. The absence of high RhoA activity in the cell body challenges the notion that RhoA regulates focal adhesion assembly in the cell body[2]. However, the conclusion in ref. 2 was reached using tools (C3-transferase, dominant-negative and dominant-positive constructs) that do not discriminate between different Rho family isoforms (RhoA, RhoB, RhoC) or their downstream signalling. It is therefore possible that some functions attributed to RhoA are due to different Rho isoforms.

We also detected high RhoA activity at the distal side of serum-induced peripheral ruffles (Fig. 3a, Supplementary Fig. S6a, b and Supplementary Movie S4; observed in 30 out of 38 ruffling events, $n = 8$ cells). RhoA activity trailed ruffles as they moved rearwards on the dorsal side of the cell, and ceased as the ruffle disappeared. This was not an artefact of cell motion between acquisition of the FRET and CFP images, as the same result was obtained with fixed cells or when the images were acquired in reverse order (data not shown). Neither was this FRET signal an artefact of ruffle thickness (Supplementary Fig. S6c), as use of a dominant-negative biosensor greatly

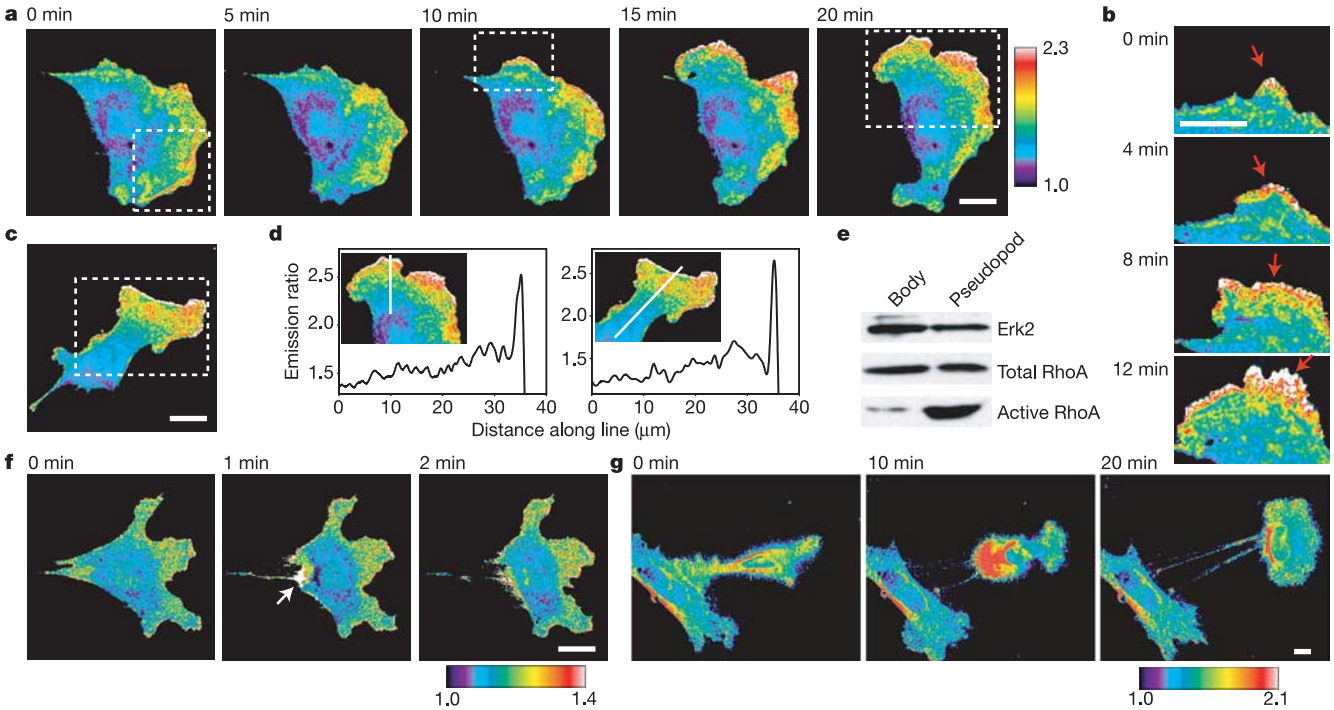

Figure 2 | RhoA activity in randomly migrating MEFs. **a**, **c**, MEFs migrating on fibronectin. **b**, Dynamics of a single protrusion from the region outlined in the $t = 10$ min frame of **a**. **d**, Emission ratio profiles along the indicated lines from insets at $t = 20$ min in **a** and in **c**. **e**, Western blot analysis of endogenous RhoA activity in purified pseudopod and cell body fractions from cells migrating in a fibronectin gradient. **f**, **g**, RhoA activation patterns during tail retraction. Images in **a**, **c** and **f** are scaled so that regions of intense RhoA activity are shown in white. Scale bars, 20 μm.

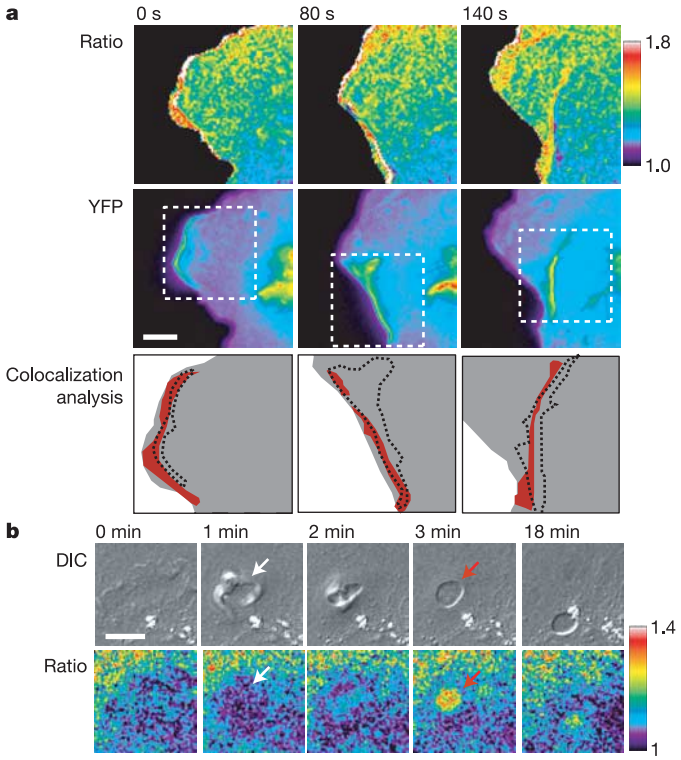

Figure 3 | RhoA activity at ruffles and pinosomes. **a**, Time-lapse images of peripheral ruffle movement induced by 10% serum. Zones of high YFP fluorescence mark ruffle location (see Supplementary Information). In the colocalization panels (from insets in the YFP images), red represents high RhoA activation and the dotted line shows ruffle position. **b**, Time-lapse images of PDGF-induced pinocytic vesicle formation. White arrows point to the absence of high RhoA activity at crown-like dorsal ruffles before pinocytic vesicle formation, red arrows point to high RhoA activity in mature pinocytic vesicles. Scale bars, 10 μm.

reduced the emission ratio associated with the ruffles (Supplementary Fig. S6d). For reasons explained in the Supplementary Information, this activation pattern suggests that RhoA is activated throughout the distal, but not the proximal, membrane sheet of the ruffle. A similar activation pattern has also been observed using a different RhoA FRET probe[16]. This polarized RhoA activity might be important for ruffle movement, and may involve RhoA-dependent relocation of the ezrin-radixin-moesin proteins[17] or mDia[16] to this location.

PDGF also stimulated peripheral ruffling with identical RhoA activation patterns (data not shown). In contrast, there was no RhoA activation at dorsal, crown-like ruffles produced during PDGF-induced formation of pinosomes (Fig. 3b and Supplementary Movie S5; 30 out of 30 crown ruffles observed, $n = 18$ cells). This implies that distinct signalling mechanisms regulate actin dynamics at different ruffling structures. RhoA was suddenly activated at the pinosomes as they formed, and remained active as the pinosomes trafficked through cells (Fig. 3b; 14 out of 23 vesicles, $n = 18$ cells). Similar to the recent observation of mDia1-dependent regulation of actin coat formation around endosomes downstream of RhoB[18], RhoA and mDia1 might regulate the bursts of actin polymerization that enable pinosome propulsion in the cytosol[19].

PDGF stimulation induced strong lamellipodial protrusions in non-motile cells (re-plated overnight in the presence of 2% serum). However, unlike the randomly migrating cells described above, these protrusions lacked intense RhoA activity at the cell edges, and showed lower RhoA activity throughout the protrusion (Fig. 4a, b and Supplementary Movie S6; observed in all of 41 protrusions, $n = 19$ cells). To support these results, we isolated pseudopods of MEFs migrating towards a gradient of PDGF, and also observed low levels of endogenous RhoA activity in the pseudopods relative to the cell body (Fig. 4c). However, in cells with impaired RhoA function (for example, expressing a dominant-negative biosensor), PDGF stimulation only partially rescued protrusion (Supplementary Movie S7), suggesting that some RhoA activity is important for PDGF-induced membrane extension. PDGF potently activates Rac[20], leading to downregulation of RhoA activity in fibroblasts[6]. We therefore tested whether active Rac could turn off RhoA activity in membrane protrusions. Expression of dominant-positive Rac Q61L tagged with monomeric red fluorescent protein (mRFP) led to the

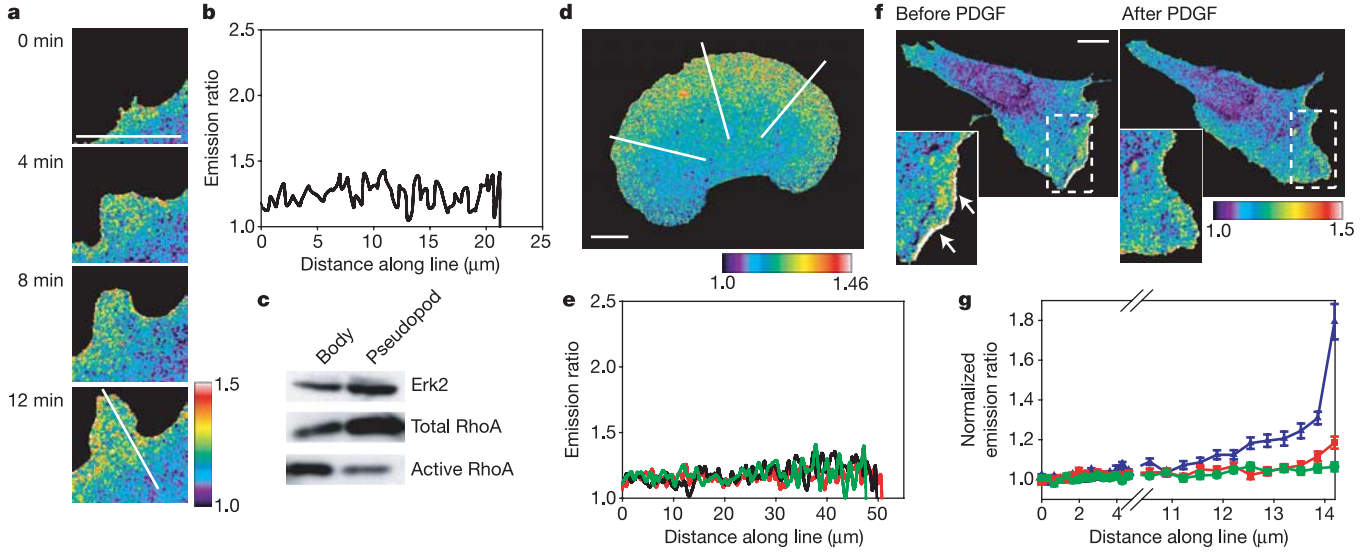

Figure 4 | PDGF-induced membrane protrusions. **a**, Dynamics of a PDGF-induced protrusion. **b**, Emission ratio profile along the line in the 12 min panel in **a**. **c**, Western blot analysis of endogenous RhoA activity in pseudopod and body fractions from cells migrating to a PDGF gradient. **d**, RhoA activity in a cell expressing dominant-positive mRFP–Rac Q61L. **e**, Emission ratio profiles along the lines in **d**. **f**, Cells migrating out of a wounded monolayer before and after treatment with PDGF. **g**, Averaged emission ratio profiles from multiple cells as in **d** (green, 15 cells, 84 lines) and **f** (blue, 7 min before PDGF, 14 cells, 43 lines; red, 7 min after PDGF, 13 cells, 45 lines). Error bars show s.d. Scale bars, 30 μm.

well-documented protrusive phenotype while recapitulating the RhoA activation pattern seen in PDGF-induced protrusion (Fig. 4d, e, g). This was also observed with a dominant-positive Rac G12V mutant (data not shown). PDGF stimulation also switched off pre-existing intense RhoA activation at the edges of MEFs migrating out of a wounded monolayer (Fig. 4f, g and Supplementary Movie S8). This data shows that PDGF stimulation and Rac activation downregulate RhoA activity specifically at the leading edge of migrating cells.

Our results show that RhoA activity is different in membrane protrusions induced by growth factor stimulation compared to that observed during random cell migration or in cells in a wounded monolayer. Antagonism between Rac and RhoA[5,6] has a prominent role at the leading edge during growth factor stimulation. These multiple mechanisms regulating membrane protrusion may provide the means to produce different modes of cell motility and polarization in response to different extracellular cues.

METHODS

Microscopy and image acquisition. MEF/3T3 fibroblasts were plated on fibronectin-coated glass coverslips ($10\,\mu g\,ml^{-1}$ fibronectin for 1 h at 37 °C, Sigma). Three-to-four hours after plating, cells were imaged in Ham's F-12K medium without phenol red (Biosource) with 10% fetal bovine serum, 25 mM HEPES and $10\,\mu g\,ml^{-1}$ oxyrase reagent (Oxyrase Inc.), in a heated closed chamber. Images were obtained using a Zeiss × 40 1.3 NA Plan NeoFluar DIC lens, a Zeiss Axiovert 100TV microscope, a Quantix CCD camera (Roper Scientific) and Metamorph software (Universal Imaging).

For emission ratio imaging, the following filter sets were used (Chroma): CFP: D436/20, D470/40; FRET: D436/20, HQ535/30; YFP: HQ500/20, HQ535/30. mRFP was imaged using HQ580/30 and HQ630/40. A dichroic mirror was custom-manufactured by Chroma for compatibility with all of these filters. Cells were illuminated with a 200 W Hg lamp through a 36% neutral density filter. At each time point, three images were recorded with the following exposure times: CFP (1 s), FRET (0.5 s), YFP (0.5 s) at binning 2 × 2 or 3 × 3. In some experiments, additional differential interference contrast (DIC) and/or mRFP pictures were also recorded.

For PDGF perfusion experiments (PDGF-BB from Sigma), a heated, open perfusion chamber (Harvard Apparatus) was used to maintain cells at 37 °C on the stage. The perfusion system consisted of a digitally controlled valve assembly regulating the perfusate, driven by gravity flow. The perfusate influx line was heated using a solution heater (Harvard Apparatus) to minimize temperature drift. Throughout the experiment, fluid flow rate was maintained at approximately $1\,ml\,min^{-1}$, preventing any effects due to sudden changes in flow rate, as demonstrated using vehicle controls. For wound-healing studies, MEFs were mixed at a 1:5 concentration ratio with MEF/3T3 cells repressed with doxycyclin, plated on fibronectin-coated coverslips at 1×10^6 cells per coverslip, and allowed to adhere for 4 h. Confluent monolayers were then wounded using a razor blade, and allowed to recover for an additional 4–5 h before observation.

Image processing. Metamorph software was used to perform image analysis. All images were first shading-corrected and background-subtracted. The FRET image, because it had the largest signal-to-noise ratio and therefore provided the best distinction between the cell and the background, was thresholded to generate a binary mask with a value of zero outside the cell and a value of one inside the cell. After multiplication by this mask, the FRET image was divided by the CFP image to yield a ratio image reflecting RhoA activation throughout the cell. A linear pseudocolour lookup table was applied, and the ratio values were normalized to the lower scale value. In each experiment, CFP and FRET images were carefully inspected to verify that all portions used to create the ratio image had a high enough signal-to-noise ratio. This was especially important in thin parts of the cell where fluorescence was low. In time-lapse experiments, CFP and YFP bleached at different rates. The ratio was corrected for bleaching using a method described elsewhere[21]. Because ruffles and cell edges can move rapidly, it was important to exclude motion artefacts; we found the same result when the order of acquisition of CFP and FRET images was reversed or when fixed cells were analysed (data not shown).

Received 4 October 2005; accepted 21 February 2006.
Published online 19 March 2006.

1. Raftopoulou, M. & Hall, A. Cell migration: Rho GTPases lead the way. *Dev. Biol.* **265,** 23–32 (2004).
2. Burridge, K. & Wennerberg, K. Rho and Rac take center stage. *Cell* **116,** 167–179 (2004).
3. Fukata, Y. *et al.* Phosphorylation of adducin by Rho-kinase plays a crucial role in cell motility. *J. Cell Biol.* **145,** 347–361 (1999).
4. Palazzo, A. F., Cook, T. A., Alberts, A. S. & Gundersen, G. G. mDia mediates Rho-regulated formation and orientation of stable microtubules. *Nature Cell Biol.* **3,** 723–729 (2001).
5. Nimnual, A. S., Taylor, L. J. & Bar-Sagi, D. Redox-dependent downregulation of Rho by Rac. *Nature Cell Biol.* **5,** 236–241 (2003).
6. Sander, E. E., ten Klooster, J. P., van Delft, S., van der Kammen, R. A. & Collard, J. G. Rac downregulates Rho activity: reciprocal balance between both GTPases determines cellular morphology and migratory behaviour. *J. Cell Biol.* **147,** 1009–1022 (1999).
7. Ren, X. D., Kiosses, W. B. & Schwartz, M. A. Regulation of the small GTP-binding protein Rho by cell adhesion and the cytoskeleton. *EMBO J.* **18,** 578–585 (1999).
8. Griesbeck, O., Baird, G. S., Campbell, R. E., Zacharias, D. A. & Tsien, R. Y. Reducing the environmental sensitivity of yellow fluorescent protein. Mechanism and applications. *J. Biol. Chem.* **276,** 29188–29194 (2001).
9. Miyawaki, A. & Tsien, R. Y. Monitoring protein conformations and interactions by fluorescence resonance energy transfer between mutants of green fluorescent protein. *Methods Enzymol.* **327,** 472–500 (2000).
10. Hoffman, G. R., Nassar, N. & Cerione, R. A. Structure of the Rho family GTP-binding protein Cdc42 in complex with the multifunctional regulator RhoGDI. *Cell* **100,** 345–356 (2000).
11. Miura, K. *et al.* ARAP1: a point of convergence for Arf and Rho signaling. *Mol. Cell* **9,** 109–119 (2002).
12. Norman, J. C. *et al.* ARF1 mediates paxillin recruitment to focal adhesions and potentiates Rho-stimulated stress fiber formation in intact and permeabilized Swiss 3T3 fibroblasts. *J. Cell Biol.* **143,** 1981–1995 (1998).
13. Cho, S. Y. & Klemke, R. L. Purification of pseudopodia from polarized cells reveals redistribution and activation of Rac through assembly of a CAS/Crk scaffold. *J. Cell Biol.* **156,** 725–736 (2002).
14. Matsumura, F., Ono, S., Yamakita, Y., Totsukawa, G. & Yamashiro, S. Specific localization of serine 19 phosphorylated myosin II during cell locomotion and mitosis of cultured cells. *J. Cell Biol.* **140,** 119–129 (1998).
15. Worthylake, R. A., Lemoine, S., Watson, J. M. & Burridge, K. RhoA is required for monocyte tail retraction during transendothelial migration. *J. Cell Biol.* **154,** 147–160 (2001).
16. Kurokawa, K. & Matsuda, M. Localized RhoA activation as a requirement for the induction of membrane ruffling. *Mol. Biol. Cell* **16,** 4294–4303 (2005).
17. Shaw, R. J., Henry, M., Solomon, F. & Jacks, T. RhoA-dependent phosphorylation and relocalization of ERM proteins into apical membrane/actin protrusions in fibroblasts. *Mol. Biol. Cell* **9,** 403–419 (1998).
18. Fernandez-Borja, M., Janssen, L., Verwoerd, D., Hordijk, P. & Neefjes, J. RhoB regulates endosome transport by promoting actin assembly on endosomal membranes through Dia1. *J. Cell Sci.* **118,** 2661–2670 (2005).
19. Merrifield, C. J. *et al.* Endocytic vesicles move at the tips of actin tails in cultured mast cells. *Nature Cell Biol.* **1,** 72–74 (1999).
20. Ridley, A. J., Paterson, H. F., Johnston, C. L., Diekmann, D. & Hall, A. The small GTP-binding protein rac regulates growth factor-induced membrane ruffling. *Cell* **70,** 401–410 (1992).
21. Hodgson, L., Nalbant, P., Shen, F. & Hahn, K. M. Imaging and photobleach correction of Mero-CBD, sensor for endogenous Cdc42 activation. *Methods Enzymol.* **406,** 140–156 (2006).

Supplementary Information is linked to the online version of the paper at www.nature.com/nature.

Acknowledgements We are grateful to G. Bokoch, P. Sun, M. Schwartz, R. Tsien, C. Der and E. Sahai for reagents, and to F. Shen for help with image analysis. This work was supported by grants from the Swiss National Science Foundation, Roche Research Foundation, Novartis and Philip Morris to O.P., and from the National Institutes of Health to K.M.H. and R.L.K.

Author Information Reprints and permissions information is available at npg.nature.com/reprintsandpermissions. The authors declare competing financial interests: details accompany the paper at www.nature.com/nature. Correspondence and requests for materials should be addressed to K.M.H. (khahn@med.unc.edu) or O.P. (pertz@ucsd.edu).